Power Supply Rejection for Common-Source Linear RF Amplifiers: Theory and Measurements

Jason T. Stauth and Seth R. Sanders

University of California, Berkeley, CA, 94720, USA

***Abstract* — This paper describes an estimation of the distortion products that arise from power supply noise mixing with the RF signal in a common-source amplifier configuration. Classical Volterra-series system analysis is extended to use on a multiple-input system and the second order supply ripple sidebands are predicted relative to the magnitudes of the input signal and supply ripple. The analysis is shown to be in good agreement with BSIM3v3 simulation and lab measurements in 180nm CMOS: ripple sidebands match within 1-2dBc for a wide range of output power.**

***Index Terms* — supply rejection, voltage ripple, DC-DC converter, power amplifier, dynamic supply, adjacent channel power ratio, power supply noise**

I. Introduction

The output spectrum of RF amplifiers is highly constrained by FCC and performance requirements, leading to tight intermodulation distortion (IMD) specifications, particularly in RF power amplifier components [1]. Traditional distortion analysis has focused on near band spectral-regrowth caused by interaction of the input signal with amplifier and component nonlinearities [1,2]. However, an additional source of spectral leakage comes from noise or voltage ripple on the power supply. As demonstrated in Fig. 1, spectral energy injected from the power supply can mix with the RF carrier and be upconverted to near-band frequencies. If the RF amplifier has insufficient power supply rejection (PSR), supply noise can degrade system performance and even cause violations of the transmit spectral mask [3]. It is important to understand the interaction of supply noise with RF amplifiers for successful design of the wireless system.

Power supply noise may be caused by a number of factors including coupling of RF and analog signals to the supply through bondwires and other parasitics, thermal noise in bandgap references, and digital switching noise. An additional source of supply noise is voltage ripple from switching regulators.

Switching regulators have been used for polar modulation of nonlinear power amplifiers (PAs), [4], and dynamic voltage biasing of linear PAs [5]. To meet strict adjacent channel leakage ratio (ACLR) requirements, it is important to understand the effect of supply ripple on the PA output spectrum.

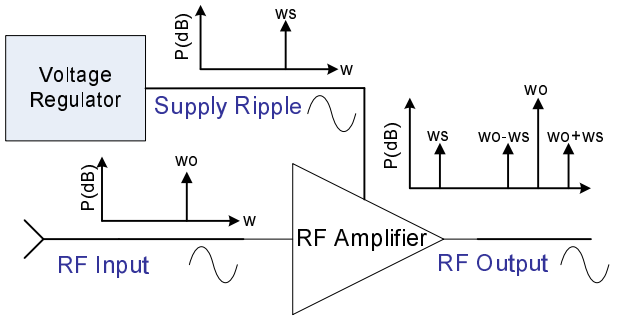

Fig. 1 Effect of supply ripple on RF amplifier output spectrum.

This work presents an analysis of the intermodulation distortion between the power supply and the RF signal for linear transconductance RF amplifiers. Calculations based on Volterra series formulation will be described that can predict low-order intermodulation terms. The analysis extends classical distortion analysis to a multi-port formulation. Specifically, this analysis is an adaptation of the method proposed by Chua in [6] and described by Wambacq and Sansen in [7]. The calculations are based on nonlinearities extracted from BSIM3v3 models, but result in expressions that are simple enough to use for hand design. Measurements are compared to hand analysis for a common source amplifier in 180nm CMOS.

Section II presents the multi-input Volterra analysis procedure. Section III describes system nonlinearities and presents Volterra operators for the supply intermodulation sidebands. Sections IV and V compare hand analysis to simulation and experimental results.

II. Theory of Multiple-Input Supply Intermodulation

A. Single-Input (Two-Port) Volterra Analysis

Volterra series can be used to analyze systems with frequency dependent nonlinearities. As long as the system is weakly nonlinear, only a few terms of the series are needed to predict important distortion phenomenon. With

a Volterra series representation, the time domain output of a nonlinear system for an input, *x(t)*, can be written as [7]:

$$y(t) = \sum_{n=0}^{\infty} F_n(x(t)), \tag{1}$$

where

$$F_n(x(t)) = \int_{-\infty}^{\infty} \cdots \int_{-\infty}^{\infty} h_n(\tau_1,\ldots,\tau_n) x(t-\tau_1)\ldots x(t-\tau_n) d\tau_1 \ldots d\tau_n . \tag{2}$$

In Equation (2), the $h_n(\tau_1,\cdots\tau_n)$ are known as the Volterra kernels of the system.

The time domain Volterra kernels can be used in the frequency domain as Volterra operators to perform circuit calculations [6],[8]. In this case the Volterra operators are frequency dependent transfer functions, $H(w_1, w_2, \cdots, w_n)$, that capture the phase and amplitude response of the circuit for a given set of frequencies.

B. Multiple-Input Volterra Analysis

The extension of 2-port Volterra analysis to multiple-input systems can be done by including both direct terms and cross terms. Volterra kernels for multiple-input systems become tensors, resulting in complicated hand calculations [6],[7]. However, hand calculation is still manageable for the low-order kernels.

The frequency domain Volterra series formulation for a system with 2 input ports and a single output may be written as:

$$\begin{aligned} So = {} & F_1(w_a)\circ S_1 + F_2(w_a,w_b)\circ S_1^{\,2} + F_3(w_a,w_b,w_c)\circ S_1^{\,3} + \ldots \\ & + G_1(w_a)\circ S_2 + G_2(w_a,w_b)\circ S_2^{\,2} + G_3(w_a,w_b,w_c)\circ S_2^{\,3} + \ldots \\ & + H_{11}(w_a,w_b)\circ (S_1 \cdot S_2) \\ & + H_{12}(w_a,w_b,w_c)\circ S_1 S_2^{\,2} + H_{21}(w_a,w_b,w_c)\circ S_1^{\,2} S_2 + \ldots \end{aligned} \tag{3}$$

Here F_i and G_i are the conventional input-output Volterra operators for each of the two input terminals. The H_{11} operator describes the second order cross term. H_{21} and H_{12} describe the third order cross terms. The operator "$\circ$" represents the frequency domain operation of the transfer function on the signal/s at the appropriate frequencies. This notation is borrowed from [9].

A three-port amplifier, such as that shown in Fig. 1, has an input port (that may be single ended or differential), a supply port, and a ground reference. In this case F_1 would correspond to the forward gain at w_0, G_1 would correspond to the forward supply noise gain at w_S, H_{11} would correspond to the first sideband at $w_O \pm w_S$, and H_{12} and H_{21} would correspond to the third order sidebands at $w_O \pm 2w_S$ and $2w_O \pm w_S$.

III. CHARACTERIZATION OF NONLINEARITIES

To study the effect of supply noise on RF amplifiers, the systematic nonlinearities are identified. For the CMOS device used in this treatment, the main sources of supply-carrier intermodulation are the transconductance, output conductance and drain-bulk junction capacitance. The body-effect transconductance, gate-source and gate-drain capacitance may also cause distortion depending on the bias point and configuration of the device.

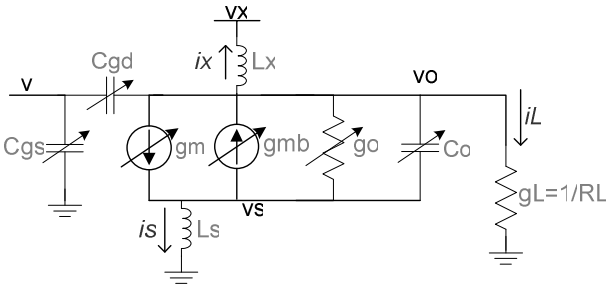

Fig. 3 Small signal model of a CMOS inductor-degenerated common source amplifier showing nonlinear elements.

Fig. 3 shows the small signal model of a common source RF amplifier. An inductive choke provides high impedance at the RF frequency, but may be low impedance at supply noise frequencies. Inductive source degeneration is included in this case to model bondwire impedance. To establish the set of Volterra operators, the drain current is expressed as a sum of nonlinear components [7]. The nonlinearities are extracted through Spectre simulation and least-squares curve fitting to match the polynomial expansion:

$$\begin{aligned} id = {} & gm_1 vgs + gm_2 vgs^{\,2} + gm_3 vgs^{\,3} + \cdots \\ & - gmb_1 vsb - gmb_2 vsb^{\,2} - gmb_3 vsb^{\,3} - \cdots \\ & + gmo_1 vds \cdot vgs + gmo_{12} vds \cdot vgs^{\,2} + gmo_{21} vds^{\,2} vgs + \cdots \\ & + go_1 vds + go_2 vds^{\,2} + go_3 vds^{\,3} + \cdots \\ & + C_1 \frac{d}{dt} vdb + \frac{C_2}{2} \frac{d}{dt} vdb^{\,2} + \frac{C_3}{3} \frac{d}{dt} vdb^{\,3} + \cdots \end{aligned} \tag{4}$$

where gm_i represents the forward transconductance, gmb_i is the body transconductance, gmo_i is the output-transconductance cross term, go_i is the output conductance, and C_i is the output capacitance.

To solve for the Volterra operators in (3), nodal equations are written and the system is solved sequentially for each order of the polynomial expansion in (4), beginning with the first order term. Source degeneration is initially neglected and the system is solved for load current, i_L. The transfer function for generation of sidebands due to supply ripple is:

$$i_L(w_0 \pm w_S) = H_{11}(w_o, w_S) \circ vi \cdot vs . \tag{5}$$

In (5), the non-symmetric transimpedance operator, H_{11}, is solved as:

$$H_{11}(w_0, w_S) = -\frac{gmo_1 G1 + 2\cdot(go_2 + jw_{sb}\frac{C_2}{2})\frac{F_1 G_1}{g_L}}{g_L + go_1 + jw_{sb}C_1 + (jw_{sb}L_X)^{-1}}. \quad (6)$$

Here F_1 and G_1 are the first order operators, and w_{sb} is the sideband frequency. The first order operators are evaluated at the corresponding input signal frequency:

$$F_1(w_0) = -\frac{gm_1 g_L}{g_L + go_1 + jw_0 C_1 + (jw_0 L_X)^{-1}}, \quad (7)$$

and

$$G_1(w_S) = \frac{g_x g_L}{g_L + go_1 + jw_S C_1 + (jw_S L_X)^{-1}}. \quad (8)$$

In (6), upconversion of supply ripple results from second order nonlinearity of the output conductance, drain junction capacitance, and dependence of the forward transconductance on v_{ds}. Source inductance degenerates the amplifier, linearizing the forward gain and reducing the ripple sidebands. The source-degenerated Volterra operators may be calculated by extending the nodal analysis to include the source terminal. In simple cases, this calculation may also be done with feedback analysis. The series-series feedback factor is calculated as the transfer function between the load current and source voltage:

$$f = -(\frac{g_L + y_X}{g_L \cdot y_S}), \quad (9)$$

where $y_x \sim (jwL_X)^{-1}$, and $y_s \sim (jwL_S)^{-1}$. The supply ripple sidebands are reduced by a factor of approximately $1+F_1(w_{sb})f(w_{sb})$, neglecting second order effects and the body transconductance. Since these effects may be important in certain circumstances, the extended nodal analysis approach is recommended for highest accuracy.

IV. Comparison to Simulation

To verify the distortion analysis, a reference design was created in 180nm CMOS. A least-squares polynomial expansion was used to match the coefficients in (3) to BSIM3v3 parameters extracted from Spectre simulation. The polynomial coefficients were used in Matlab to estimate the Volterra operators and the resulting distortion products.

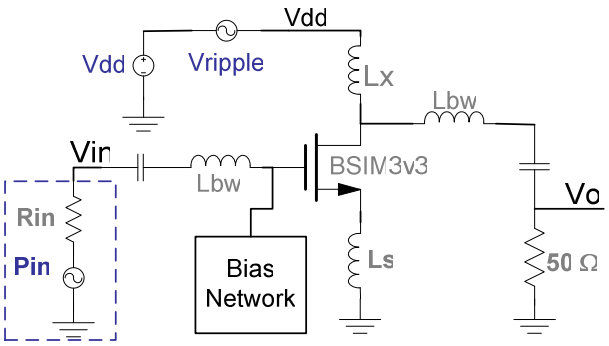

Fig. 4 Spectre/BSIM simulation model

Fig. 4 shows a schematic representation of the Spectre simulation model. A supply voltage of 1.8V is used with 50mV voltage ripple amplitude at w_S = 10MHz. Source inductance of 0.5nH is included to represent inductance of the ground path including bond wires. Inductance of the input/output path, *Lbw*, was simulated at ~1.0nH. The input RF voltage magnitude was swept between 1mV and 316mV at a carrier frequency of 900MHz.

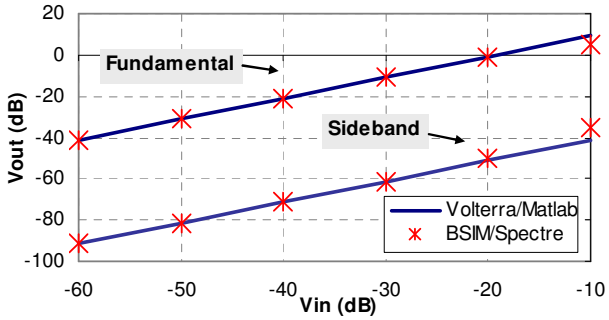

Fig. 5 Comparison of Spectre simulation to calculations

Fig. 5 shows a comparison of the Matlab-Volterra analysis to simulation with Spectre and BSIM3v3 models. The Volterra analysis predicts the magnitude of the output spectrum at w_0 and $w_O \pm w_S$ within 0.5dB for signals below the compression point of the amplifier.

V. Comparison to Measurement

The reference design from the previous example was fabricated in a test IC to compare to hand analysis. The amplifier and biasing networks were placed on chip. Matching and impedance transformation networks were designed at the board level. Estimates were made of the bond wire parasitics to include in the hand analysis. The measurement setup included an RF source, spectrum analyzer, and waveform generator to inject supply ripple.

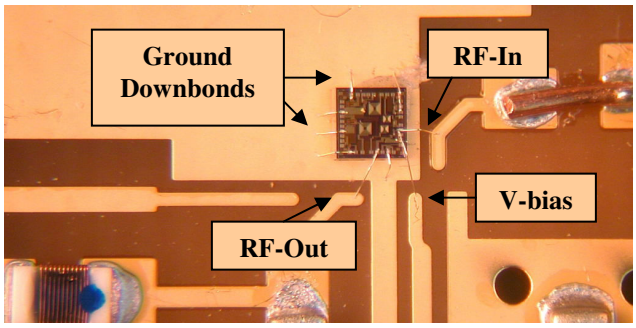

Fig. 7 Photograph of the die bonded on the gold-plated test board. Die area is 1.4mmX1.4mm.

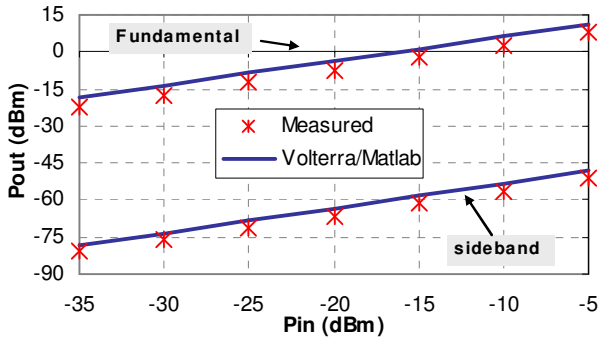

Fig. 9 Comparison of measured and calculated fundamental and ripple sideband power; 50mV supply ripple at 10MHz.

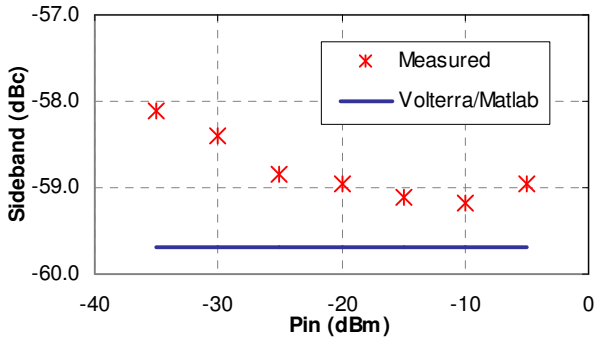

Fig. 10 Comparison of measured and calculated ripple sideband in decibles-below carrier.

A photo of the test IC bonded to the board is shown in Fig. 7. Fig. 9 compares measured results to hand analysis. Trends in spectral leakage due to supply ripple are in good agreement with hand analysis. However, absolute power measurements for the fundamental and ripple sidebands are shifted by ~2-3dB from hand predictions. The discrepancy is caused by losses in the output passives, connectors and cabling that are not included in simulation.

A more important comparison, the sideband power referenced in decibels-below-carrier (dBc) to the fundamental, is shown in Fig. 10. In this case, sideband power is seen to match hand analysis within 2dB over a wide (30dB) output power range. This demonstrates that hand analysis can have reasonable success in predicting the effect of supply noise relative to the output power of the amplifier.

VI. Conclusion

A method of predicting the interaction of power supply noise with the RF carrier was presented and compared to measured data. Classical 2-port Volterra-series distortion analysis was extended to a multi-port formulation to predict supply ripple sidebands. Relative measurement of ripple sideband power showed agreement within 1-2dBc of prediction. This analysis provides a tool to study the power supply rejection of RF amplifiers. Such analysis can help RF designers predict output spectrum, and may be valuable when spectral leakage and ACPR specifications are of critical importance.

Acknowledgement

The authors would like to thank Panasonic and the U.C. Micro program for financial support and Dr. Ali Niknejad for his helpful comments and advice.

References

[1] J. Vuolevi and T. Rahkonen, *Distortion in RF power amplifiers*. Boston: Artech House, 2003.

[2] B. Baytekin and R. Meyer, "Analysis and simulation of spectral regrowth in radio frequency power amplifiers," *IEEE Journal of Solid State Circuits*, vol. 40, no. 2, pp. 370-381, Feb. 2005.

[3] H. Kobayashi and P. Asbeck, "Active Cancellation of Switching Noise for DC-DC Converter-Driven RF Power Amplifiers," Microwave Symposium Digest MTT-S, vol. 3, pp. 1647-1650, 2002.

[4] T. Oshmia and M. Kokubo, "Simple polar-loop transmitter for dual-mode bluetooth," *IEEE International Symposium on Circuits and Systems (ISCAS)*, vol. 4, pp. 3966-3969, May 2005.

[5] G. Hanington, P.-F. Chen, P. Asbeck, and L. E. Larson, "High-efficiency power amplifier using dynamic power-supply voltage for CDMA applications," *IEEE Transactions on Microwave Theory and Techniques*, vol. 47, pp. 1471-1476, Aug. 1999.

[6] L. O. Chua and N. C.-Y., "Frequency-domain analysis of nonlinear systems: formulation of transfer functions," *IEE Journal on Electronic Circuits and Systems*, vol. 3, no. 6, pp. 257-269, Nov. 1979.

[7] P. Wambacq and W. M. C. Sansen, *Distortion analysis of analog integrated circuits*. Boston, Mass: Kluwer Academic, 1998.

[8] M. Schetzen, *The Volterra and Wiener theories of nonlinear systems*. New York: Wiley, 1980.

[9] R. Meyer, "EECS 242 course notes." University of California, Berkeley, Spring 2004.